HHS Public Access

Author manuscript

J Comp Neurol. Author manuscript; available in PMC 2016 September 01.

Published in final edited form as:

J Comp Neurol. 2015 September 1; 523(13): 1913–1924. doi:10.1002/cne.23770.

Organization of TNIK in dendritic spines

Alain C. Burette[1,*], **Kristen D. Phend**[1], **Susan Burette**[1], **Qingcong Lin**[3], **Musen Liang**[4], **Gretchen Foltz**[5], **Noël Taylor**[6], **Qi Wang**[7], **Nicholas J. Brandon**[8], **Brian Bates**[9], **Michael D. Ehlers**[7], and **Richard J. Weinberg**[1,2]

[1]Dept of Cell Biology & Physiology, University of North Carolina, Chapel Hill, NC, USA

[2]Neuroscience Center, University of North Carolina, Chapel Hill, NC, USA

[3]Shenogen Pharma Group Ltd., Beijing, PRC

[4]Department of Pharmacokinetics, Dynamics, and Metabolism Pfizer, Andover, MA, USA

[5]Clinical Research Unit, Pfizer, New Haven, CT, USA

[6]Biomarker and Personalized Medicine Group Eisai Product Creation Systems Eisai, Inc, Andover MA, USA

[7]Neuroscience Research Unit, Pfizer Cambridge, MA, USA

[8]AstraZeneca Neuroscience IMED, Cambridge, MA, USA

[9]Centers for Therapeutic Innovation, Pfizer, Boston, MA, USA

Abstract

TRAF2- and NCK-interacting kinase (TNIK) has been identified as an interactor of the psychiatric risk factor, Disrupted in Schizophrenia 1 (DISC1). As a step toward deciphering its function in the brain, we performed high-resolution light and electron microscopic immunocytochemistry. We demonstrate here that TNIK is expressed in neurons throughout the adult mouse brain. In striatum and cerebral cortex, TNIK concentrates in dendritic spines, especially in the vicinity of the lateral edge of the synapse. Thus, TNIK is highly enriched at a microdomain critical for glutamatergic signaling and implicated in the regulation of synaptic strength.

Keywords

TNIK; dendritic spine; PSD; cerebral cortex; striatum RRID:AB_11212843; RRID:AB_1858225; RRID:AB_11213019; RRID:nif-0000-30467; RRID:AB_94396

TRAF2- and NCK-interacting kinase (TNIK) is a serine/threonine kinase of the Ste20 family (Fu et al., 1999; Taira et al., 2004). In addition to its enzymatic activity, TNIK also

[*]Correspondence to: Alain Burette, Dept. of Cell Biology & Physiology CB# 7090, University of North Carolina, Chapel Hill, NC 27599, alain.burette@gmail.com.

Conflict of interest statement

BB, QW, MDE, ML, GF, QL, NT are/were employees and/or shareholders of Pfizer, Inc. The other authors verify that they have no known or potential conflict of interest including any financial, personal, or other relationships with other people or organizations within 3 years of beginning the submitted work that could inappropriately influence, or be perceived to influence, this work.

contains scaffolding domains, raising the possibility that TNIK also acts as a scaffold that assembles molecular complexes for downstream signal transduction. TNIK was originally cloned from a human brain cDNA library, and its message is found at particularly high levels in the brain (Fu et al., 1999). Genetic association studies, as well as transcription profiling of blood and postmortem brain, support a role for TNIK as a risk factor for several psychiatric diseases, including bipolar disorder, attention deficit-hyperactivity disorder, and schizophrenia (Glatt et al., 2005; Matigian et al., 2007; Potkin et al., 2009; Shi et al., 2009; Ayalew et al., 2012; Elia et al., 2012). Moreover, TNIK binds to the well-known psychiatric risk factor DISC1 (Camargo et al., 2007; Wang et al., 2011; Coba et al., 2012).

Proteomic studies consistently find that TNIK protein is in the biochemically-defined postsynaptic density (PSD) (Jordan et al., 2004; Peng et al., 2004; Collins et al., 2006; Trinidad et al., 2008; Hussain et al., 2010; Wang et al., 2011), where it has been implicated in postsynaptic signaling (Hussain et al., 2010; Wang et al., 2011; Coba et al., 2012). Knockdown experiments in cultured primary neurons point to a role for TNIK in promoting surface expression of the AMPA-type glutamate receptor subunit GluR1 (Hussain et al., 2010; Wang et al., 2011). This effect may be related to the finding that TNIK can stabilize the levels of several other PSD proteins, including the scaffold protein PSD-95 and the transmembrane AMPA receptor regulatory protein γ-2, stargazin (Wang et al., 2011). TNIK is also linked to the NMDA receptor, via the A-kinase anchoring protein 9 (Yotiao), and activation of NMDA receptors and group I metabotropic glutamate receptors can modify TNIK phosphorylation (Coba et al., 2012).

To gain further insight into the neurobiology of TNIK, we have studied its localization in the brain of adult mouse, focusing on neocortex and striatum, two regions of particular interest in human neuropsychiatric disease.

MATERIALS AND METHODS

Animals

All procedures related to the care and treatment of animals were in accordance with institutional and NIH guidelines; all animals use protocols were reviewed and approved by the relevant Institutional Animal Care and Use Committee.

To generate TNIK knockout animal, a targeting vector containing 6.2 and 6.3 kb of genomic DNA 5′ and 3′ respectively of the targeted modification was constructed. A loxP site 5′ and a PGK promoter-neo^{R}-LoxP cassette 3′ of exon 7 was introduced into this construct, thereby flanking exon7 with LoxP sites (Fig. 1A). C57BL/6NTac ES cells were targeted using standard procedures, and appropriately targeted clones were identified by Southern blotting using genomic probes outside of the targeting vector on both the 5′ and 3′ sides. Appropriate incorporation of the LoxP site 5′ of exon 7 was confirmed by PCR.

Targeted ES cells were used to establish this modification in the C57BL/6NTac mouse strain by standard procedures. Exon 7, which encodes 43 amino acids of the kinase domain, was removed by crossing mice carrying the targeted allele to a protamine-cre recombinase transgenic. In these C57BL/6NTac transgenics, Cre recombinase is expressed in the male

germline, allowing animals bearing a fully recombined allele lacking exon 7 in all tissues to be derived. Subsequent breeding eliminated the transgene and established the recombined allele lacking exon 7, referred to as TNIK$^{\Delta 7}$, in the germline.

TNIK mRNA was detected in whole brain mRNA by RT-PCR using the following primer sets: Forward primer (exon 6) 5′-GGCCTGAGTCACCTGCACCAGC-3′; Reverse primer (exon 8) 5′-GGGCACCTTCTGCCATCTCA-3′ (Fig. 1B). TNIK$^{\Delta 7}$/TNIK$^{\Delta 7}$ homozygous mice showed a residual transcript in which exon 6 was spliced to exon 8, resulting in the introduction of 2 stop codons within the next 30 nucleotides after the novel 6/8 splice site.

Fully inbred C57BL/6NTac homozygous TNIK$^{\Delta 7}$/TNIK$^{\Delta 7}$ and wild type littermates were generated for this study by intercross of heterozygotes (+/TNIK$^{\Delta 7}$).

Antibody specificity

Table 1 provides a list of primary antibodies used in this study.

To identify TNIK we used a rabbit polyclonal antibody (Sigma-Aldrich Cat# HPA012297 RRID:AB_1858225) raised against human TNIK. To verify antibody specificity, we performed immunocytochemistry on brain sections from TNIK KO mice, run in parallel with sections from control mice. Staining with HPA012297 antibody was robust in tissue from WT mice, but extremely weak in tissue from TNIK$^{\Delta 7}$/TNIK$^{\Delta 7}$ mice, exhibiting a “background” pattern unrelated to that seen for WT brain sections (Fig. 1C, D). Three additional TNIK antibodies were also tested: MC-7403 (MBL International, Woburn, MA), PA5-15181 (Thermo Fisher Scientific Cat# PA5-15181 RRID:AB_2207637), and HPA012128 (Sigma-Aldrich Cat# HPA012128 RRID:AB_1858226). Using MC-7403, PA5-15181 and HPA012128 (at a range of dilutions: 1:100 to 1:10,000), similar patterns of staining were observed for both WT and TNIK$^{\Delta 7}$/TNIK$^{\Delta 7}$ tissues; thus, these antibodies were not suitable for immunohistochemistry. Accordingly, HPA012297 was used for all data presented in this paper.

To identify the vesicular glutamate transporter VGLUT1, we used a guinea pig polyclonal antibody (Chemicon, Millipore Corporation, Billerica, MA, AB5905, lot# 24041061, RRID:AB_11213019) raised against rat VGLUT1. We have previously sequenced the immunogenic peptide (Chemicon, Millipore Corporation, Billerica, MA, #AG208), concluding that this antibody was raised against a C-terminal peptide (GATHSTVQPPRPPPPVRDY, (Melone et al., 2005)). The antibody recognizes a single band of ~ 60 KDa on immunoblots of synaptic membrane fractions from rat cerebral cortex. Furthermore, immunogold labeling shows that VGLUT1 immunoreactivity is selectively associated with axon terminals forming asymmetric synapses in cerebral cortex and hippocampus.

To identify GABAergic synapses, we use a mouse monoclonal antibody raised against GABA conjugated to BSA (Millipore Cat# MAB316, RRID:AB_94396, lot # 2080836, Millipore Corporation, Billerica, MA). This antibody does not cross-react with other amino acids.

For choline acetyltransferase (ChAT), a goat polyclonal antibody was used (Chemicon, cat. # AG208, RRID:AB_11212843). The antibody recognizes ChAT on Western blots, and immunostaining was not observed in tissue sections when the antiserum was preadsorbed with pure ChAT protein (Bruce et al., 1985; Shiromani et al., 1987). Furthermore, this antibody produced labeling that was similar to labeling produced by the well-characterized monoclonal antibody AB8 (Armstrong et al., 1983; Levey et al., 1983).

Tissue preparation

After inducing deep anesthesia with sodium pentobarbital (60 mg/kg, i.p.), mice were intracardially perfused with 50–100 ml of fixative: 4% freshly-depolymerized paraformaldehyde in phosphate buffer (PB, 0.1 M, pH 7.4) for light microscopy (LM); a mixture of 4% paraformaldehyde and 0.1% glutaraldehyde in PB, for LM labeling with GABA; or a mixture of 2% paraformaldehyde and 2% glutaraldehyde in PB for post-embedding electron microscopy (EM). Brains were sectioned at 50 μm and 100 μm on a Vibratome, and collected in cold PB.

Light microscopic immunohistochemistry

Free-floating sections were incubated in 10% normal donkey serum (NDS). The primary antibody (TNIK, 1:1000) was then applied overnight. For immunoperoxidase microscopy, sections were then incubated for 3 hours in biotinylated secondary antibody (1:200; Jackson ImmunoResearch, West Grove, PA) and for 1 hour in ExtrAvidin-peroxidase complex (1:5,000; Sigma, St. Louis, MO); peroxidase was histochemically visualized with nickel-intensified diaminobenzidine. Processed sections were mounted on gelatin-coated slides, air dried, and cleared with xylene before being coverslipped with D.P.X. mountant (BDH Chemicals, Poole, England).

For immunofluorescence microscopy, antigenic sites were visualized with donkey IgG conjugated to DyLight 549 (1:200, Jackson ImmunoResearch; West Grove, PA). For double labeling, the second primary antibody (1:5,000, guinea pig anti-VGLUT1, 1:5,000, mouse anti-GABA or 1:2,000 goat anti-ChAT) was applied overnight and visualized by a secondary antibody conjugated to Alexa 488 (1:200, Invitrogen). Some sections were then counterstained with Hoechst 33342 (Sigma, St. Louis, MO) to visualize nuclei and NeuroTrace 640-660 (Invitrogen, Thermo Fisher Scientific, Rockford, IL) to selectively visualize neuronal somata. Control experiments, in which the primary antibodies were omitted, were performed to control for nonspecific binding of the secondary antibody. Sections were examined with a Leitz DMR microscope (Leica, Wetzlar, Germany), and a Leica SP2 confocal microscope.

Electron microscopic immunocytochemistry

Brain sections (100 μm) were pre-treated in 0.1% calcium chloride in 0.1 M sodium acetate, rinsed, and cryoprotected in a graded series to 30% glycerol in 0.1 M sodium acetate. Sections were quick-frozen in methanol chilled with dry ice. Freeze substitution in 4% uranyl acetate in methanol was carried out in a Leica Automatic Freeze Substitution System; after rinsing in methanol, sections were infiltrated with Lowicryl HM-20, mounted between sheets of ACLAR plastic sandwiched between glass slides, and polymerized with ultraviolet

light. After polymerization, regions of interest were cut from the sections and glued to plastic blocks. Sections were cut at ~70–90 nm with an ultramicrotome and collected on nickel grids, coated with Coat-Quick (Electron Microscopy Sciences). Grids were pre-treated 15 minutes at 60 °C in 0.01 M citrate buffer, pH 6, rinsed in water, blocked in 1% bovine serum albumin in TRIS-buffered saline with 0.005% Tergitol NP-10, then incubated overnight at 21–24°C with the primary antibody (TNIK, HPA012297, 1:1000). Grids were rinsed, blocked in 1% normal goat serum, and incubated in goat anti-rabbit IgG F(ab)2 conjugated to 10-nm gold particles (1:20, Ted Pella, Redding, CA). Grids were then rinsed and counterstained with 1% uranyl acetate, followed by Sato's lead, and examined in a Philips Tecnai electron microscope (Hillsboro, OR) at 80 kV.

Image analysis

To further test TNIK antibody specificity for postembedding EM immunohistochemisty, and to evaluate the distribution of labeling in different subcellular compartments, we collected random EM photomontages (each ~ 10 × 10 μm) from neuropil of the cerebral cortex from WT and KO mice. We used ImageJ (Schneider et al., 2012) (ImageJ, RRID:nif-0000-30467) to outline all identifiable dendritic spines, PSDs, presynaptic terminals, mitochondria and dendritic shafts. Since these were from single sections, many profiles, especially neuroglial processes and the smallest axons and dendrites, could not be unambiguously identified, and were therefore excluded from further analysis. We then computed the density of gold particles for each compartment, analyzing tissue from WT and KO mice in a blinded fashion.

To investigate the organization of immunogold label associated with the PSD of asymmetric synapses (likely for their morphology to be glutamatergic), we took measurements from 35–40 immunolabeled synapses for each of the two brain regions studied, from each of three animals. To define "axodendritic" position, the shortest distance between the center of each gold particle and the outer leaflet of the postsynaptic membrane was measured. To define the "lateral" synaptic position of a gold particle along the synapse, we measured the distance from each end of the PSD to a line drawn perpendicular to the synaptic apposition, running through the center of the particle (Valtschanoff and Weinberg, 2001). Normalized lateral position of each gold particle within the axodendritic peak (from −10 nm to +50 nm from the postsynaptic membrane) was computed as $L_N = |(a-b)|/(a+b)$, where a and b are tangential distances along the plasma membrane from the center of the gold particle to the lateral edges of the synaptic specialization; thus $L_N = 0$ for gold particles at the center of the PSD, and $L_N = 1$ for particles at its edge.

RESULTS

Immunoperoxidase-reacted sections displayed staining for TNIK in the grey matter throughout the brain; with little or no immunostaining in the white matter (Fig. 2A). TNIK staining was strong in olfactory bulb (2B), piriform cortex (2C), isocortex (2D), hippocampus (2E), striatum (2F), thalamus (2G), hypothalamus (2H) and cerebellum (2I). Immunostaining was weaker in midbrain, pons, and medulla. We focused our attention on

neocortex and striatum, two brain regions implicated in multiple human psychiatric disorders.

TNIK was expressed through all layers of the neocortex, most prominent in layer II (Fig. 2D); no obvious differences in the pattern of labeling were seen across neocortical areas. TNIK was detected in somata and dendrites, and in small puncta throughout the neuropil. Counterstaining with NeuroTrace (a fluorescent Nissl stain) and Hoechst 33342 (a nuclear stain) showed that TNIK was generally restricted to neurons. Most neuronal somata throughout the neocortex contained TNIK (Fig. 3A–H), although scattered somata exhibited little or no staining (arrows in Fig. 3E–H). Our suspicion that these might represent inhibitory interneurons was confirmed by double labeling with GABA, which showed that most GABA-positive somata were immunonegative for TNIK (Fig. 3I–K).

In the striatum, TNIK was prominently expressed in the gray matter between fascicles of myelinated fibers, which themselves were devoid of staining (Fig. 4). TNIK staining was strong in somata and dendrites of cells likely for their number, size, and distribution to be medium spiny neurons; numerous puncta in the neuropil were also staining. Scattered larger somata exhibited little or no TNIK staining. Double labeling with choline acetyltransferase (ChAT) showed that most of these TNIK-negative neurons were large aspiny cholinergic interneurons (Fig. 4I–K).

In both cortex and striatum, TNIK was excluded from the nucleus. Immunostaining within the somatic cytoplasm was typically organized into patches or blobs; many of these blobs colocalized with Nissl bodies (as defined by Neurotrace), suggesting an association of TNIK with rough endoplasmic reticulum (Fig. 3E–H; Fig. 4E–H. TNIK staining was weak and diffuse in dendrites, which consequently were barely visible. It was our impression that in many cases these dendrites were “coated” with brightly-stained puncta. Abundant punctate TNIK staining was present throughout the neuropil in both neocortex and striatum. Double labeling experiments revealed a close relationship between these puncta and the presynaptic marker VGLUT1 (Fig. 5), suggesting an association of TNIK with excitatory synapses in both cortex (whose spiny principal neurons are glutamatergic) and striatum (whose spiny principal neurons are GABAergic).

In summary, TNIK in the forebrain was expressed mainly in spiny neurons, especially at puncta likely to represent glutamatergic synapses.

To elucidate the organization of TNIK in the vicinity of the synapse, we analyzed its distribution with electron microscopy, using postembedding immunogold labeling (Fig. 6). Gold particles coding for TNIK labeled somata and dendrites, concentrating in dendritic spines; particles were only occasionally seen in presynaptic terminals. In spines, TNIK labeling concentrated over the PSD. Labeling was also detected within the cytoplasm of the spine head, though at lower concentrations. To ensure that the preferential PSD labeling seen here reflected the distribution of antigen, rather than simply arising from nonspecific adsorption to the protein-rich environment of the synapse, we performed the same immunogold analysis on tissue from $TNIK^{\Delta 7}/TNIK^{\Delta 7}$ mice.

Labeling over the protein-rich mitochondria was twice as high in the $TNIK^{\Delta 7}/TNIK^{\Delta 7}$ as in WT material (Table 2). We interpret this staining as nonspecific, and have often encountered similar nonspecific labeling over mitochondria in other postembedding immunocytochemical studies. In contrast, the density of gold particles over the PSD was more than 6-fold higher in WT than in $TNIK^{\Delta 7}/TNIK^{\Delta 7}$ tissue, implying that at least 85% of the staining at the PSD of WT mice represented genuine TNIK protein (Table 2). Labeling densities in dendritic spines and shafts were also higher in the WT than in $TNIK^{\Delta 7}/TNIK^{\Delta 7}$, though background noise in the face of a weaker signal made interpretation difficult. Quantification of label densities in different subcellular compartments showed that label over the PSD was enriched by a factor of at least 60, compared to the entire neuropil, consistent with the high levels of enrichment seen in biochemical PSD fractions (Wang et al., 2011). We conclude that TNIK is indeed expressed at high levels within the anatomical domain of the PSD.

To better define the spatial organization of TNIK in the PSD, we measured the distance of synapse-associated immunogold particles to the plasma membrane. We found that labeling for TNIK concentrated very close to the postsynaptic membrane, lying at a mean distance of 6 nm inside the membrane, in both neocortex and striatum (Fig. 6D). To determine the tangential distribution of TNIK along the length of PSD, we computed the “normalized lateral position” (L_N) of gold particles along the membrane (confining our attention to particles lying within a window between −10 nm and +50 nm from the postsynaptic plasma membrane, to restrict attention to label associated with the PSD). We found that TNIK labeling in both neocortex and striatum concentrated in the vicinity of the lateral edge of the PSD (Fig. 6E). The striatum, but not cortex, also exhibited a peak of label (~21% of the total synaptic pool) at the center of the PSD (Fig. 6E).

DISCUSSION

We used immunohistochemistry to examine the distribution of TNIK in the mouse brain. The protein was widely expressed in neurons and neuropil throughout the gray matter; in somata it was excluded from the nuclear compartment. Focusing on cerebral cortex and striatum, we found that TNIK concentrates in the dendritic spines of principal neurons (where it associates with the postsynaptic density), whereas local circuit interneurons (including GABAergic neurons in cortex and cholinergic neurons in striatum) often failed to stain above background. At least some of the somatic labeling likely reflected newly-synthesized protein awaiting transport, but we cannot exclude that TNIK may also play a functional role in the cytoplasm.

In model systems, TNIK interacts with the adhesion and signaling molecule β-catenin to modulate cell proliferation via the canonical Wnt signaling pathway (Mahmoudi et al., 2009; Satow et al., 2010; Shitashige et al., 2010; Schurch et al., 2012). In contrast to this well-documented effect in cancer biology and in normal embryonic development, the role of TNIK in the adult brain is poorly understood. Impaired neurogenesis has been reported in TNIK KO mice (Coba et al., 2012), suggesting that TNIK may also be important for cell proliferation in the brain. However, the presence of TNIK in excitatory synapses points to a role beyond neurogenesis.

The present results show that TNIK in spines concentrates at the lateral edge of the PSD in both excitatory pyramidal cells of cerebral cortex and inhibitory medium spiny neurons (MSNs) of striatum; TNIK also concentrated in the PSD center in synapses onto MSNs, but not in synapses onto pyramidal cells. This result, along with previous data suggesting differences in the organization of PSD proteins between the excitatory spiny cells of cortex and hippocampus and the inhibitory spiny cells of striatum (Kharazia et al., 1996; Kharazia and Weinberg, 1997; Bernard and Bolam, 1998; Clarke and Bolam, 1998; Racca et al., 2000; Burette et al., 2014), raise the possibility that there may be fundamental differences in synaptic structure between glutamatergic synapses onto excitatory vs inhibitory neurons.

Notwithstanding this subtle difference, TNIK in both types of synapses concentrates mainly at the peripheral edge of the PSD. This lateral “perisynaptic” zone is also a preferential target for the actin filaments that link the synapse to the spine core (Frost et al., 2010; Svitkina et al., 2010; Burette et al., 2012). The perisynaptic zone plays a special role in the trafficking of AMPA receptors (Lu et al., 2007; Petrini et al., 2009; Freche et al., 2011), which represents a principal mechanism underlying long-term synaptic plasticity. Evidence from both knockdown experiments and knockout mice shows that disruption of TNIK impairs AMPAR signaling (Hussain et al., 2010; Wang et al., 2011; Coba et al., 2012), apparently via activation of Rap2, a regulator of the actin cytoskeleton (Hussain et al., 2010; Coba et al., 2012); TNIK may also regulate actin by phosphorylating the actin-binding protein gelsolin (Fu et al., 1999).

We find that TNIK lies very close to the plasma membrane, where it can interact with integral membrane proteins (Valtschanoff and Weinberg, 2001), especially those concentrating at the edge of the synapse. Intriguingly, the cadherin/catenin complex is also enriched at synapses (Benson and Tanaka, 1998; Togashi et al., 2002), especially in the perisynaptic zone (Uchida et al., 1996; Petralia et al., 2005; Petralia et al., 2010). Besides its role in synapse assembly and dendritic spine formation, this complex is involved in actin remodeling, and also regulates synaptic AMPARs (Nuriya and Huganir, 2006; Okuda et al., 2007; Silverman et al., 2007; Tai et al., 2008; Peng et al., 2009; Brigidi and Bamji, 2011). This correspondence in both location and function leads us to speculate that TNIK at the synapse is linked to β-catenin.

Pathologies in both neocortex and striatum are strongly implicated in psychiatric disease. Especially considering TNIK’s association with AMPA receptors, with actin signaling pathways, and with DISC1 (variants of which have been linked to multiple psychiatric diseases), we suggest that that understanding the biology of TNIK represents an important avenue of research to understand psychiatric illness.

Acknowledgments

Grant support: The work is supported by Pfizer Inc. and R01 NS039444 (RJW)

Imaging was supported by the Michael Hooker Microscopy Facility.

Role of authors

Design and construction of the TNIK$^{\Delta 7}$/TNIK$^{\Delta 7}$ mice: QL, ML, GF, NT, QW, NJB, BB. Histology and immunohistochemistry AB, SB, KP. Data acquisition and analysis: AB. Drafting of the manuscript: AB. Final manuscript preparation: AB, RJW. Obtained funding: RJW, MDE

References

Armstrong DM, Saper CB, Levey AI, Wainer BH, Terry RD. Distribution of cholinergic neurons in rat brain: demonstrated by the immunocytochemical localization of choline acetyltransferase. J Comp Neurol. 1983; 216(1):53–68. [PubMed: 6345598]

Ayalew M, Le-Niculescu H, Levey DF, Jain N, Changala B, Patel SD, Winiger E, Breier A, Shekhar A, Amdur R, Koller D, Nurnberger JI, Corvin A, Geyer M, Tsuang MT, Salomon D, Schork NJ, Fanous AH, O'Donovan MC, Niculescu AB. Convergent functional genomics of schizophrenia: from comprehensive understanding to genetic risk prediction. Molecular psychiatry. 2012; 17(9): 887–905. [PubMed: 22584867]

Benson DL, Tanaka H. N-cadherin redistribution during synaptogenesis in hippocampal neurons. The Journal of neuroscience: the official journal of the Society for Neuroscience. 1998; 18(17):6892–6904. [PubMed: 9712659]

Bernard V, Bolam JP. Subcellular and subsynaptic distribution of the NR1 subunit of the NMDA receptor in the neostriatum and globus pallidus of the rat: co-localization at synapses with the GluR2/3 subunit of the AMPA receptor. Eur J Neurosci. 1998; 10(12):3721–3736. [PubMed: 9875351]

Brigidi GS, Bamji SX. Cadherin-catenin adhesion complexes at the synapse. Current opinion in neurobiology. 2011; 21(2):208–214. [PubMed: 21255999]

Bruce G, Wainer BH, Hersh LB. Immunoaffinity purification of human choline acetyltransferase: comparison of the brain and placental enzymes. Journal of neurochemistry. 1985; 45(2):611–620. [PubMed: 4009177]

Burette AC, Lesperance T, Crum J, Martone M, Volkmann N, Ellisman MH, Weinberg RJ. Electron tomographic analysis of synaptic ultrastructure. J Comp Neurol. 2012; 520(12):2697–2711. [PubMed: 22684938]

Burette AC, Park H, Weinberg RJ. Postsynaptic distribution of IRSp53 in spiny excitatory and inhibitory neurons. J Comp Neurol. 2014; 522(9):2164–2178. [PubMed: 24639075]

Camargo LM, Collura V, Rain JC, Mizuguchi K, Hermjakob H, Kerrien S, Bonnert TP, Whiting PJ, Brandon NJ. Disrupted in Schizophrenia 1 Interactome: evidence for the close connectivity of risk genes and a potential synaptic basis for schizophrenia. Molecular psychiatry. 2007; 12(1):74–86. [PubMed: 17043677]

Clarke NP, Bolam JP. Distribution of glutamate receptor subunits at neurochemically characterized synapses in the entopeduncular nucleus and subthalamic nucleus of the rat. J Comp Neurol. 1998; 397(3):403–420. [PubMed: 9674565]

Coba MP, Komiyama NH, Nithianantharajah J, Kopanitsa MV, Indersmitten T, Skene NG, Tuck EJ, Fricker DG, Elsegood KA, Stanford LE, Afinowi NO, Saksida LM, Bussey TJ, O'Dell TJ, Grant SG. TNiK is required for postsynaptic and nuclear signaling pathways and cognitive function. The Journal of neuroscience: the official journal of the Society for Neuroscience. 2012; 32(40):13987–13999. [PubMed: 23035106]

Collins MO, Husi H, Yu L, Brandon JM, Anderson CN, Blackstock WP, Choudhary JS, Grant SG. Molecular characterization and comparison of the components and multiprotein complexes in the postsynaptic proteome. Journal of neurochemistry. 2006; 97(Suppl 1):16–23. [PubMed: 16635246]

Elia J, Glessner JT, Wang K, Takahashi N, Shtir CJ, Hadley D, Sleiman PM, Zhang H, Kim CE, Robison R, Lyon GJ, Flory JH, Bradfield JP, Imielinski M, Hou C, Frackelton EC, Chiavacci RM, Sakurai T, Rabin C, Middleton FA, Thomas KA, Garris M, Mentch F, Freitag CM, Steinhausen HC, Todorov AA, Reif A, Rothenberger A, Franke B, Mick EO, Roeyers H, Buitelaar J, Lesch KP, Banaschewski T, Ebstein RP, Mulas F, Oades RD, Sergeant J, Sonuga-Barke E, Renner TJ, Romanos M, Romanos J, Warnke A, Walitza S, Meyer J, Palmason H, Seitz C, Loo SK, Smalley SL, Biederman J, Kent L, Asherson P, Anney RJ, Gaynor JW, Shaw P, Devoto M, White PS, Grant SF, Buxbaum JD, Rapoport JL, Williams NM, Nelson SF, Faraone SV, Hakonarson H. Genome-wide copy number variation study associates metabotropic glutamate receptor gene

networks with attention deficit hyperactivity disorder. Nature genetics. 2012; 44(1):78–84. [PubMed: 22138692]

Freche D, Pannasch U, Rouach N, Holcman D. Synapse geometry and receptor dynamics modulate synaptic strength. PloS one. 2011; 6(10):e25122. [PubMed: 21984900]

Frost NA, Shroff H, Kong H, Betzig E, Blanpied TA. Single-molecule discrimination of discrete perisynaptic and distributed sites of actin filament assembly within dendritic spines. Neuron. 2010; 67(1):86–99. [PubMed: 20624594]

Fu CA, Shen M, Huang BC, Lasaga J, Payan DG, Luo Y. TNIK, a novel member of the germinal center kinase family that activates the c-Jun N-terminal kinase pathway and regulates the cytoskeleton. The Journal of biological chemistry. 1999; 274(43):30729–30737. [PubMed: 10521462]

Glatt SJ, Everall IP, Kremen WS, Corbeil J, Sasik R, Khanlou N, Han M, Liew CC, Tsuang MT. Comparative gene expression analysis of blood and brain provides concurrent validation of SELENBP1 up-regulation in schizophrenia. Proceedings of the National Academy of Sciences of the United States of America. 2005; 102(43):15533–15538. [PubMed: 16223876]

Hussain NK, Hsin H, Huganir RL, Sheng M. MINK and TNIK differentially act on Rap2-mediated signal transduction to regulate neuronal structure and AMPA receptor function. The Journal of neuroscience: the official journal of the Society for Neuroscience. 2010; 30(44):14786–14794. [PubMed: 21048137]

Jordan BA, Fernholz BD, Boussac M, Xu C, Grigorean G, Ziff EB, Neubert TA. Identification and verification of novel rodent postsynaptic density proteins. Molecular & cellular proteomics: MCP. 2004; 3(9):857–871. [PubMed: 15169875]

Kharazia VN, Phend KD, Rustioni A, Weinberg RJ. EM colocalization of AMPA and NMDA receptor subunits at synapses in rat cerebral cortex. Neuroscience letters. 1996; 210(1):37–40. [PubMed: 8762186]

Kharazia VN, Weinberg RJ. Tangential synaptic distribution of NMDA and AMPA receptors in rat neocortex. Neuroscience letters. 1997; 238(1–2):41–44. [PubMed: 9464650]

Levey AI, Armstrong DM, Atweh SF, Terry RD, Wainer BH. Monoclonal antibodies to choline acetyltransferase: production, specificity, and immunohistochemistry. The Journal of neuroscience: the official journal of the Society for Neuroscience. 1983; 3(1):1–9. [PubMed: 6822847]

Lu J, Helton TD, Blanpied TA, Racz B, Newpher TM, Weinberg RJ, Ehlers MD. Postsynaptic positioning of endocytic zones and AMPA receptor cycling by physical coupling of dynamin-3 to Homer. Neuron. 2007; 55(6):874–889. [PubMed: 17880892]

Mahmoudi T, Li VS, Ng SS, Taouatas N, Vries RG, Mohammed S, Heck AJ, Clevers H. The kinase TNIK is an essential activator of Wnt target genes. The EMBO journal. 2009; 28(21):3329–3340. [PubMed: 19816403]

Matigian N, Windus L, Smith H, Filippich C, Pantelis C, McGrath J, Mowry B, Hayward N. Expression profiling in monozygotic twins discordant for bipolar disorder reveals dysregulation of the WNT signalling pathway. Molecular psychiatry. 2007; 12(9):815–825. [PubMed: 17440432]

Melone M, Burette A, Weinberg RJ. Light microscopic identification and immunocytochemical characterization of glutamatergic synapses in brain sections. J Comp Neurol. 2005; 492(4):495–509. [PubMed: 16228991]

Nuriya M, Huganir RL. Regulation of AMPA receptor trafficking by N-cadherin. Journal of neurochemistry. 2006; 97(3):652–661. [PubMed: 16515543]

Okuda T, Yu LM, Cingolani LA, Kemler R, Goda Y. beta-Catenin regulates excitatory postsynaptic strength at hippocampal synapses. Proceedings of the National Academy of Sciences of the United States of America. 2007; 104(33):13479–13484. [PubMed: 17679699]

Peng J, Kim MJ, Cheng D, Duong DM, Gygi SP, Sheng M. Semiquantitative proteomic analysis of rat forebrain postsynaptic density fractions by mass spectrometry. The Journal of biological chemistry. 2004; 279(20):21003–21011. [PubMed: 15020595]

Peng YR, He S, Marie H, Zeng SY, Ma J, Tan ZJ, Lee SY, Malenka RC, Yu X. Coordinated changes in dendritic arborization and synaptic strength during neural circuit development. Neuron. 2009; 61(1):71–84. [PubMed: 19146814]

Petralia RS, Sans N, Wang YX, Wenthold RJ. Ontogeny of postsynaptic density proteins at glutamatergic synapses. Molecular and cellular neurosciences. 2005; 29(3):436–452. [PubMed: 15894489]

Petralia RS, Wang YX, Hua F, Yi Z, Zhou A, Ge L, Stephenson FA, Wenthold RJ. Organization of NMDA receptors at extrasynaptic locations. Neuroscience. 2010; 167(1):68–87. [PubMed: 20096331]

Petrini EM, Lu J, Cognet L, Lounis B, Ehlers MD, Choquet D. Endocytic trafficking and recycling maintain a pool of mobile surface AMPA receptors required for synaptic potentiation. Neuron. 2009; 63(1):92–105. [PubMed: 19607795]

Potkin SG, Turner JA, Guffanti G, Lakatos A, Fallon JH, Nguyen DD, Mathalon D, Ford J, Lauriello J, Macciardi F, Fbirn. A genome-wide association study of schizophrenia using brain activation as a quantitative phenotype. Schizophrenia bulletin. 2009; 35(1):96–108. [PubMed: 19023125]

Racca C, Stephenson FA, Streit P, Roberts JD, Somogyi P. NMDA receptor content of synapses in stratum radiatum of the hippocampal CA1 area. The Journal of neuroscience: the official journal of the Society for Neuroscience. 2000; 20(7):2512–2522. [PubMed: 10729331]

Satow R, Shitashige M, Jigami T, Honda K, Ono M, Hirohashi S, Yamada T. Traf2- and Nck-interacting kinase is essential for canonical Wnt signaling in Xenopus axis formation. The Journal of biological chemistry. 2010; 285(34):26289–26294. [PubMed: 20566648]

Schneider CA, Rasband WS, Eliceiri KW. NIH Image to ImageJ: 25 years of image analysis. Nature methods. 2012; 9(7):671–675. [PubMed: 22930834]

Schurch C, Riether C, Matter MS, Tzankov A, Ochsenbein AF. CD27 signaling on chronic myelogenous leukemia stem cells activates Wnt target genes and promotes disease progression. The Journal of clinical investigation. 2012; 122(2):624–638. [PubMed: 22232214]

Shi J, Levinson DF, Duan J, Sanders AR, Zheng Y, Pe'er I, Dudbridge F, Holmans PA, Whittemore AS, Mowry BJ, Olincy A, Amin F, Cloninger CR, Silverman JM, Buccola NG, Byerley WF, Black DW, Crowe RR, Oksenberg JR, Mirel DB, Kendler KS, Freedman R, Gejman PV. Common variants on chromosome 6p22.1 are associated with schizophrenia. Nature. 2009; 460(7256):753–757. [PubMed: 19571809]

Shiromani PJ, Armstrong DM, Bruce G, Hersh LB, Groves PM, Gillin JC. Relation of pontine choline acetyltransferase immunoreactive neurons with cells which increase discharge during REM sleep. Brain research bulletin. 1987; 18(3):447–455. [PubMed: 3580914]

Shitashige M, Satow R, Jigami T, Aoki K, Honda K, Shibata T, Ono M, Hirohashi S, Yamada T. Traf2- and Nck-interacting kinase is essential for Wnt signaling and colorectal cancer growth. Cancer research. 2010; 70(12):5024–5033. [PubMed: 20530691]

Silverman JB, Restituito S, Lu W, Lee-Edwards L, Khatri L, Ziff EB. Synaptic anchorage of AMPA receptors by cadherins through neural plakophilin-related arm protein AMPA receptor-binding protein complexes. The Journal of neuroscience: the official journal of the Society for Neuroscience. 2007; 27(32):8505–8516. [PubMed: 17687028]

Svitkina T, Lin WH, Webb DJ, Yasuda R, Wayman GA, Van Aelst L, Soderling SH. Regulation of the postsynaptic cytoskeleton: roles in development, plasticity, and disorders. The Journal of neuroscience: the official journal of the Society for Neuroscience. 2010; 30(45):14937–14942. [PubMed: 21068295]

Tai CY, Kim SA, Schuman EM. Cadherins and synaptic plasticity. Current opinion in cell biology. 2008; 20(5):567–575. [PubMed: 18602471]

Taira K, Umikawa M, Takei K, Myagmar BE, Shinzato M, Machida N, Uezato H, Nonaka S, Kariya K. The Traf2- and Nck-interacting kinase as a putative effector of Rap2 to regulate actin cytoskeleton. The Journal of biological chemistry. 2004; 279(47):49488–49496. [PubMed: 15342639]

Togashi H, Abe K, Mizoguchi A, Takaoka K, Chisaka O, Takeichi M. Cadherin regulates dendritic spine morphogenesis. Neuron. 2002; 35(1):77–89. [PubMed: 12123610]

Trinidad JC, Thalhammer A, Specht CG, Lynn AJ, Baker PR, Schoepfer R, Burlingame AL. Quantitative analysis of synaptic phosphorylation and protein expression. Molecular & cellular proteomics: MCP. 2008; 7(4):684–696. [PubMed: 18056256]

Uchida N, Honjo Y, Johnson KR, Wheelock MJ, Takeichi M. The catenin/cadherin adhesion system is localized in synaptic junctions bordering transmitter release zones. The Journal of cell biology. 1996; 135(3):767–779. [PubMed: 8909549]

Valtschanoff JG, Weinberg RJ. Laminar organization of the NMDA receptor complex within the postsynaptic density. The Journal of neuroscience: the official journal of the Society for Neuroscience. 2001; 21(4):1211–1217. [PubMed: 11160391]

Wang Q, Charych EI, Pulito VL, Lee JB, Graziane NM, Crozier RA, Revilla-Sanchez R, Kelly MP, Dunlop AJ, Murdoch H, Taylor N, Xie Y, Pausch M, Hayashi-Takagi A, Ishizuka K, Seshadri S, Bates B, Kariya K, Sawa A, Weinberg RJ, Moss SJ, Houslay MD, Yan Z, Brandon NJ. The psychiatric disease risk factors DISC1 and TNIK interact to regulate synapse composition and function. Molecular psychiatry. 2011; 16(10):1006–1023. [PubMed: 20838393]

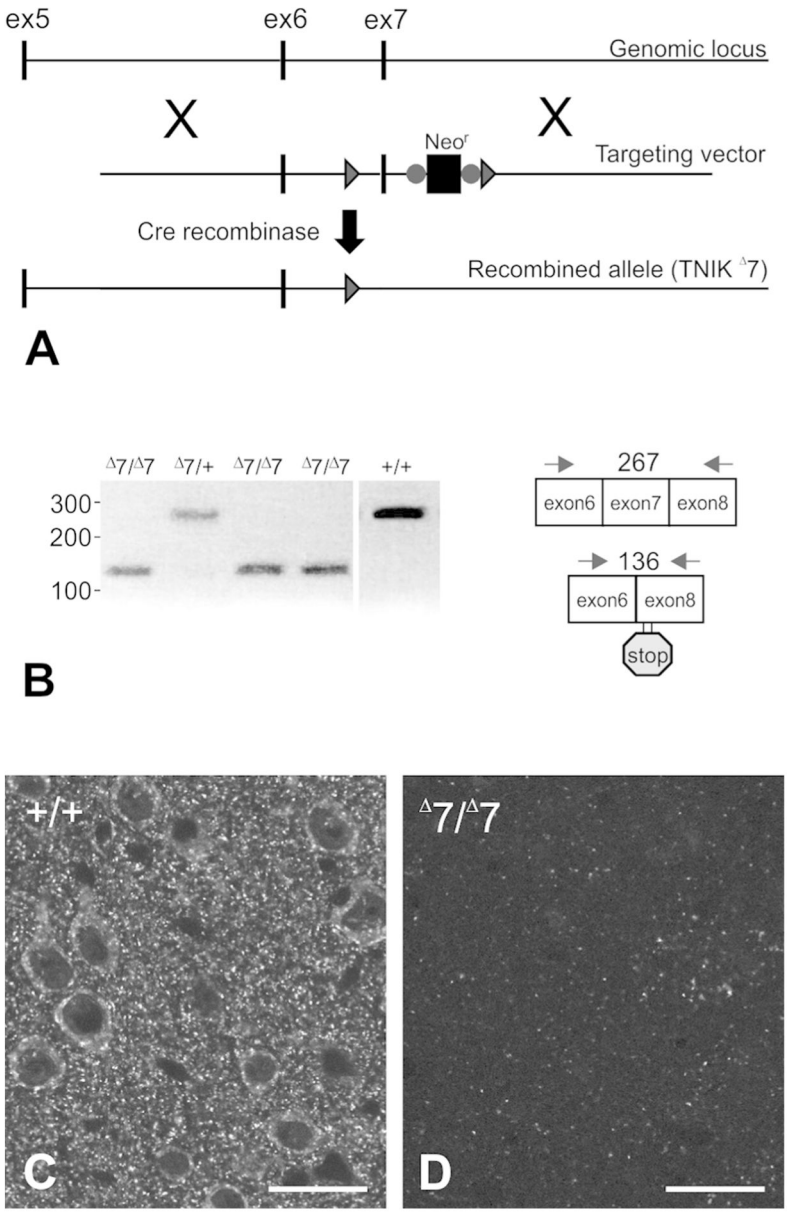

Figure 1. Preparation of the knockout mice

A: Gene targeting of TNIK locus and RT-PCR of whole brain mRNA from targeted mice. Genomic locus illustrating the region of exons 5–7. Targeting vector indicated showing homology arms, LoxP sites flanking exon 7 (▶), and neomycin (G418) resistance cassette used for selection. Neo^r cassette is flanked by Frt sites (●). After introduction into the germline, exon 7 was removed by Cre recombinase-mediated deletion. **B**: RT-PCR of whole brain RNA from animals of the indicated genotypes. PCR primers located in exons 6 and 8 indicated by arrows. Deletion of exon 7 results in a novel transcript in animals carrying the Δ7 allele that contains early termination codons as indicated. Identity of PCR products was verified by sequencing (data not shown). **C**: Immunofluorescence staining for TNIK in neocortex from WT (**A**) and TNIK$^{\Delta 7}$/TNIK$^{\Delta 7}$ (**B**) mouse brain.

Scale bar = 50 μm in C and D.

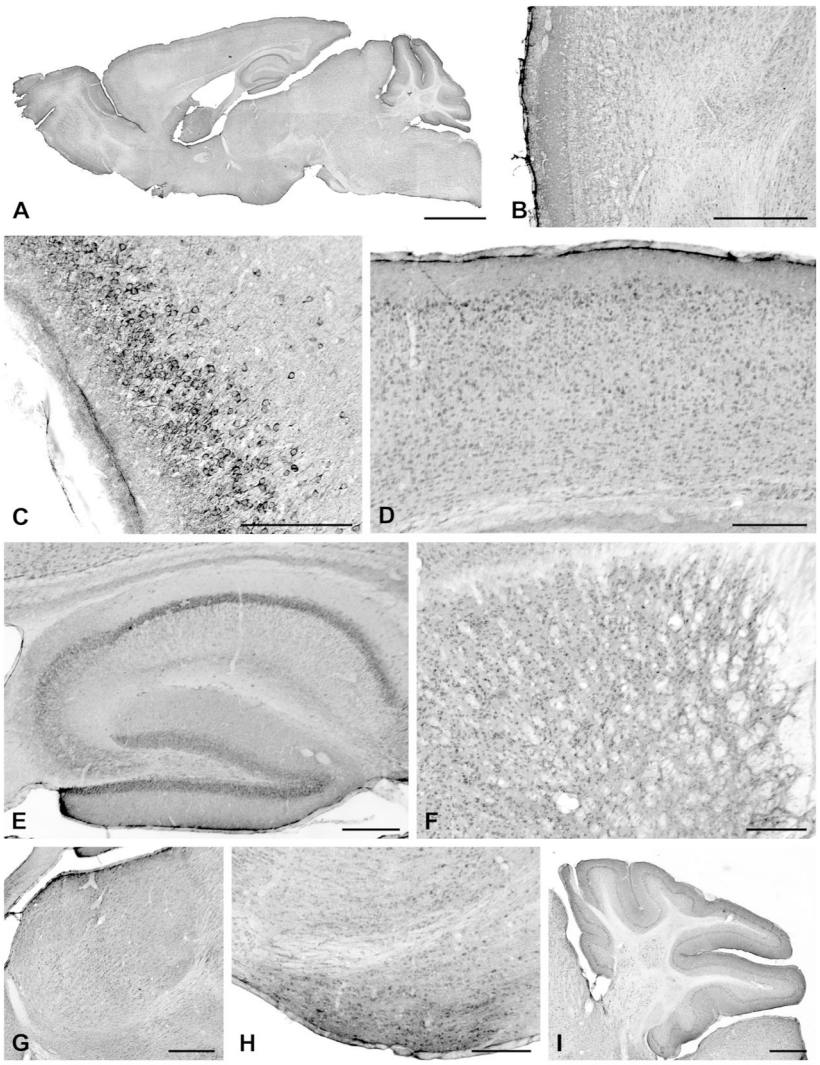

Figure 2. Immunoperoxidase staining for TNIK in the mouse brain

A: Parasagittal section of whole mouse brain. Staining is conspicuous in gray matter, largely sparing white matter. Higher magnification views show patterns of staining in specific regions of brain, including **B**: Olfactory bulb; **C**: Piriform cortex; **D**: Neocortex; **E**: Hippocampus; **F**: Striatum; **G**: Thalamus; **H**: Hypothalamus; **I**: Cerebellum.

Scale bar = 2 mm in A; 500 μm in B, 200 μm in C; 250 μm in D, E, F; 500 μm in G; 250 μm in H; 500 μm in I.

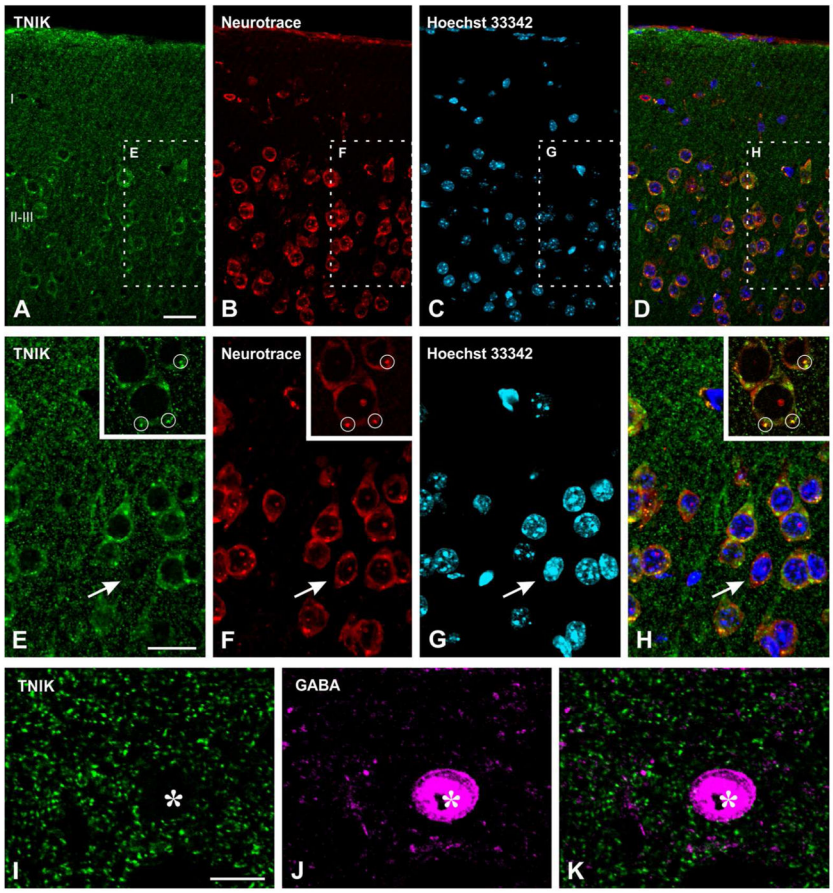

Figure 3. Immunofluorescence labeling for TNIK in neocortex

A–D: Sections were counterstained with Hoechst 33342 to visualize nuclei, and with NeuroTrace 640-660 to visualize neuronal somata. Most NeuroTrace-identified neurons are also immunopositive for TNIK, though to varying degrees. **E–H**: Enlargement of boxed area from upper panel; white arrow points to a small neuron immunonegative for TNIK (extended-focus confocal images). Insets: enlarged single-focus images from the same field; note that many somatic TNIK "blobs" in **E** correspond to Nissl bodies as defined by Neurotrace (**F**); some examples are outlined with white circles. **I–K**; Double labeling for TNIK and GABA; a GABAergic soma (asterisk) is immunonegative for TNIK.
Scale bar = 30 μm in A–D; 20 μm in E–H; 10 μm in I–K.

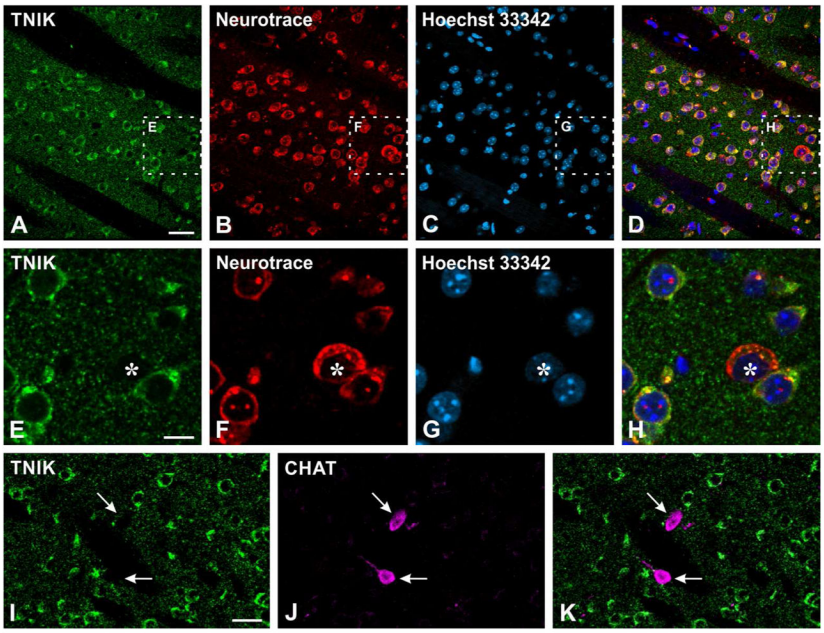

Figure 4. Immunofluorescence labeling for TNIK in striatum

A–H: Sections were counterstained with Hoechst 33342 to visualize nuclei, and NeuroTrace 640-660 to visualize neuronal somata. Most neurons in the field were immunopositive for TNIK. Boxed area in upper panel is shown at higher magnification in middle panel (**E–H**). The asterisk marks a neuron immunonegative for TNIK. **I–K**: Double labeling for TNIK and ChAT; white arrows point to ChAT-positive neurons that are immunonegative for TNIK. Scale bar = 30 μm in A–D; 10 μm in E–H; 25 μm in I–K.

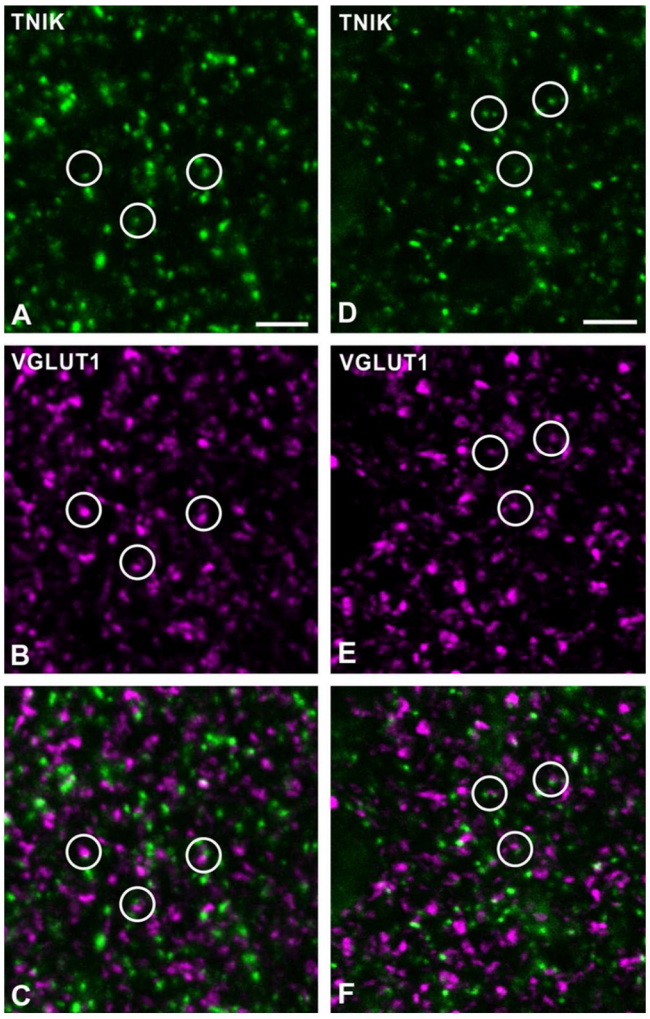

Figure 5. Colocalization of TNIK with VGLUT1

Double labeling in mouse neocortex (**A–C**) and striatum (**D–F**) shows that many TNIK puncta (green) are closely apposed to, or partially overlap with, the vesicular glutamate transporter VGLUT1 (magenta), suggesting that TNIK concentrates at synapses. Scale bar = 4 μm in A–F.

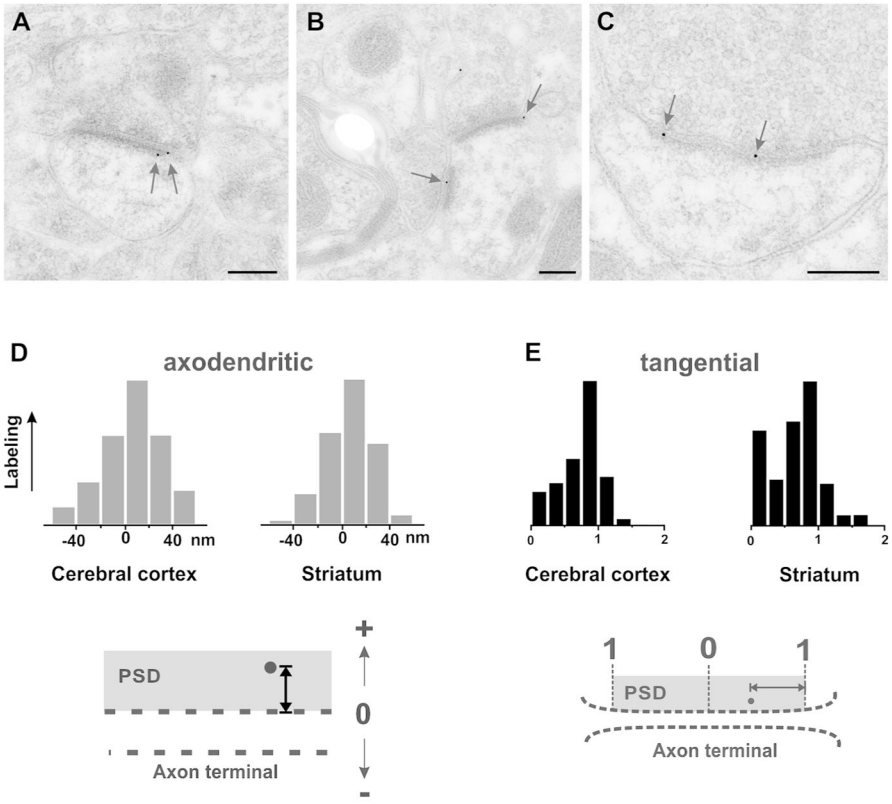

Figure 6. Ultrastructural analysis using postembedding immunogold electron microscopy reveals association of TNIK with the postsynaptic density (PSD)

A: an immunopositive spine in cerebral cortex; arrows point to two particles lying close to the edge of the PSD. **B**: micrograph shows a thin dendritic shaft in cortex receiving two asymmetric synapses; both are immunopositive for TNIK. The lower arrow points to a gold particle lying in the middle of the synapse, whereas the upper arrow points to a particle lying at the edge of the PSD. **C**: view of a large immunopositive spine in striatum; two gold particles (arrows) lie close to the postsynaptic membrane. **D**: histograms show the distribution of immunolabeling in the axodendritic axis (20 nm bins, cerebral cortex: N=135 synaptic particles, striatum: N=133 particles). Diagram at bottom illustrates measurement technique; positive values correspond to particles lying inside the postsynaptic plasma membrane. The pattern of labeling was consistent for cortex (left) and striatum (right), peaking just inside the postsynaptic membrane. **E**: histograms show distribution of label tangentially along the synapse, normalized such that 0 corresponds to the center of the PSD, and 1.0 to its edge (see diagram at bottom; cortex: N=120 synaptic particles, striatum N=116 particles). Labeling in both cortex (left) and striatum (right) concentrated in the vicinity of the edge of the PSD. An additional pool of TNIK lay at the center of the PSD in striatum, but not in cortex. X-axis for each histogram has been normalized so that the largest bin corresponds to 1.0 units, and the origin corresponds to zero.

Scale bar = 200 nm in A, B, C

Table 1

Primary Antibodies

Antigen	Immunogen	Source	Dilution
ChAT	Human placental choline acetyltransferase	Chemicon, AB144, RRID:AB_11212843	1:2,000
GABA	GABA conjugated to BSA	Millipore Corporation, clone 5A9, Cat. # MAB316, lot # 2080836	1:5,000
TNiK	Synthetic peptide from internal domain of human TNiK aa 809-933.	SIGMA Cat# HPA012297, RRID:AB_1858225	1:1,000
VGLUT1	C-terminal peptide rat VGLUT1: GATHSTVQPPRPPPPVRDY	Chemicon, cat. # AG208, RRID:AB_11213019	1:5,000

Table 2

	WT	KO	WT/KO
PSDs	32.16 ± 4.81	5.32 ± 0.71	6.1
Spines	0.86 ± 0.40	0.42 ± 0.19	2.0
Dendritic shafts	0.38 ± 0.07	0.26 ± 0.02	1.5
Axon terminals	0.55 ± 0.24	0.52 ± 0.17	1.0
Mitochondria	1.49 ± 0.36	3.06 ± 0.36	0.5

Number of gold particles/μm^2